Available online at www.sciencedirect.com
ScienceDirect
Trans. Nonferrous Met. Soc. China 22(2012) 2471−2476
Transactions of Nonferrous Metals Society of China
www.tnmsc.cn

Selective synthesis and shape-dependent photoluminescence properties of $(Y_{0.95}Eu_{0.05})_2O_3$ submicron spheres and microplates

ZHU Qi, LI Ji-guang, XU Yong, LI Xiao-dong, SUN Xu-dong

Key Laboratory for Anisotropy and Texture of Materials of Ministry of Education, Northeastern University, Shenyang 110819, China

Received 9 July 2012; accepted 1 August 2012

Abstract: Red-emission $(Y_{0.95}Eu_{0.05})_2O_3$ submicron spheres and microplates were selectively obtained via hydrothermal precursor synthesis (150 °C, 12 h) followed by calcination at 1000 °C. Characterizations of the products were carried out by combined means of XRD, FT-IR, FE-SEM and PL analysis. The precursors could be modulated from basic-carbonate submicron spheres to normal carbonate microplates by increasing the molar ratio of urea to Y+Eu from 10 to 40−100. The resultant oxides largely retain their respective precursor morphologies at 1000 °C, but morphology confined crystal growth was observed for the microplates, yielding more enhanced exposure of the (400) facets. Both the $(Y_{0.95}Eu_{0.05})_2O_3$ spheres and microplates exhibit nearly identical positions of the PL bands and similar asymmetry factors of luminescence [$I(^5D_0\rightarrow{}^7F_2)/I(^5D_0\rightarrow{}^7F_1)$, ~11] under 250 nm excitation, but the microplates show a significantly strong red emission at ~613 nm (~1.33 times that of the spheres) owing to their larger particle size and denser packing of primary phosphor crystallites.

Key words: optical material; powder processing; morphology-dependent physical phenomena; rare earths; optical spectroscopy

1 Introduction

Eu^{3+} doped Y_2O_3 solid solution (Y_2O_3:Eu^{3+}) exhibits a sharp red emission at ~610 nm arising from the $^5D_0\rightarrow{}^7F_2$ intra-4f electronic transitions of the Eu^{3+} ions, upon short UV excitation into the charge transfer (CT) band at ~250 nm or under electron beam irradiation. The luminescent performance of a phosphor powder is known to be influenced by several factors, such as size, shape, and crystallinity of the particles. Over the past decades, a few of techniques have been developed for Y_2O_3:Eu^{3+} synthesis owing to its technological importance, such as combustion [1], sol−gel [2], high temperature pyrolysis [3,4], and thermal plasma processing [5,6], and much effort has been paid to particle size, particle shape, and crystallinity control of the products. Recently, a variety of novel Y_2O_3:Eu^{3+} nanostructures have been successfully produced, including monospheres [7−9], nanotubes [10], nanowires [11], nanorods [12], nanobelts [13,14], nanosheets [15], and microflowers [16].

It should be noted that a tunable morphology synthesis by a simple technique is of great importance but frequently remains a challenge in the field of particle science and engineering. In the present work, we selectively synthesized submicron spheres and microplates of $(Y_{0.95}Eu_{0.05})_2O_3$ phosphors by calcining their precursors autoclaved from mixed nitrate solutions containing urea. Based upon characterizations by combined techniques of XRD, FT-IR, FE-SEM, and PL analysis, the effects of processing parameter on precursor characteristics as well as morphology-dependent crystallization and luminescence behaviors of the oxides were discussed.

2 Experimental

2.1 Powder synthesis

The yttrium and europium sources for particle synthesis were Y_2O_3 (99.99% purity, Huizhou Ruier Rare-Chem. Hi-Tech. Co. Ltd., Huizhou, China) and Eu_2O_3 (99.99% purity, Conghua Jianfeng Rare Earth Co.

Foundation item: Projects (50172030, 50972025, 50990303, 51172038) supported by the National Natural Science Foundation of China; Project supported by the Liaoning BaiQianWan Talents Program, China; Projects (N110802001, N100702001) supported by the Fundamental Research Funds for the Central Universities, China; Project supported by the China Scholarship Council

Corresponding author: LI Ji-guang; Tel: +86-24-83687787; Fax: +86-24-23906316; E-mail: lijg@smm.neu.edu.cn

DOI: 10.1016/S1003-6326(11)61487-8

Ltd., Conghua, China), respectively. The other reagents were of analytical grade and were purchased from Shenyang Chemical Reagent Factory (Shenyang, China). Stock solutions of $M(NO_3)_3$ (M=Y and Eu) were prepared by dissolving the above oxides with a proper amount of hot nitric acid. The luminescence quenching concentration of Eu^{3+} in Y_2O_3 is widely observed to be ~5% (mole fraction), and thus in this work the molar ratio of Y to Eu was kept a constant of 19:1 for each run of the experiment. In a typical synthesis, a proper amount of urea was dissolved in 60 mL of 1 mmol $M(NO_3)_3$ stock solution, and the resultant mixture, after being constantly stirred for 30 min, was then transferred into a Teflon lined stainless-steel autoclave of 100 mL capacity. The autoclave was tightly sealed and was then put in an electric oven preheated to 150 °C. After 12 h of reaction, the autoclave was left to cool naturally to room temperature, and the hydrothermal product was collected via centrifugation. The wet precipitate was washed with distilled water three times to remove the byproducts, rinsed with absolute ethanol, and was finally dried in air at 100 °C for 2 h to yield a white precursor powder for further characterizations. The red phosphor Y_2O_3:Eu^{3+} was obtained by calcining the precursor in air at 1000 °C for 4 h with a heating rate of 10 °C/min at the ramp stage. The molar ratio of urea to total cation (R, R= urea/(Y+Eu)) was widely varied to investigate its influence on powder properties.

2.2 Characterization

Phase identification was performed by X-ray diffractometry (XRD, Model PW3040/60, Philips, Eindhoven, The Netherlands) operating at 40 kV/40 mA using nickel filtered Cu K_α radiation and a scanning speed of 4.0 (°)/min. Fourier transform infrared spectroscopy (FTIR, Model Spectrum RXI, Perkin-Elmer, Shelton, CT, USA) of the precursors was performed by the standard KBr method. Morphologies of the products were observed via field emission scanning electron microscopy (FE-SEM， Model JSM−7001F, JEOL, Tokyo, Japan). Photoluminescence (PL) spectra of the resultant Y_2O_3:Eu^{3+} phosphor were measured using an LS−55 fluorescence spectrophotometer (Perkin-Elmer, Shelton, CT) at room temperature.

3 Results and discussion

3.1 Effects of molar ratio of urea to Y+Eu on phase and morphology of precursor

Particle morphology of the precursor was found to be closely related to the molar ratio of urea to Y+Eu. Figure 1 shows the FE-SEM morphologies for three typical samples. At a low R value of 10, the product consists of loosely-agglomerated uniform spheres with a diameter of ~120 nm (Fig. 1(a)), showing a morphology very similar to that of the lanthanide basic carbonates classically made via urea-based homogeneous precipitation from open reaction systems under magnetic stirring [7−9]. Though in the present work, reactions proceeded under a closed hydrothermal system and without stirring. MATIJEVIĆ and HSU [17] have also produced monospheres of $Y(OH)CO_3$ via reaction at 90 °C for 2 h in capped test tubes and under a relatively low molar ratio of urea to Y of ~33. At higher R values of 40, 60 and 100, the hydrothermal products are all microplates having sections of up to ~35 μm × 5 μm, as

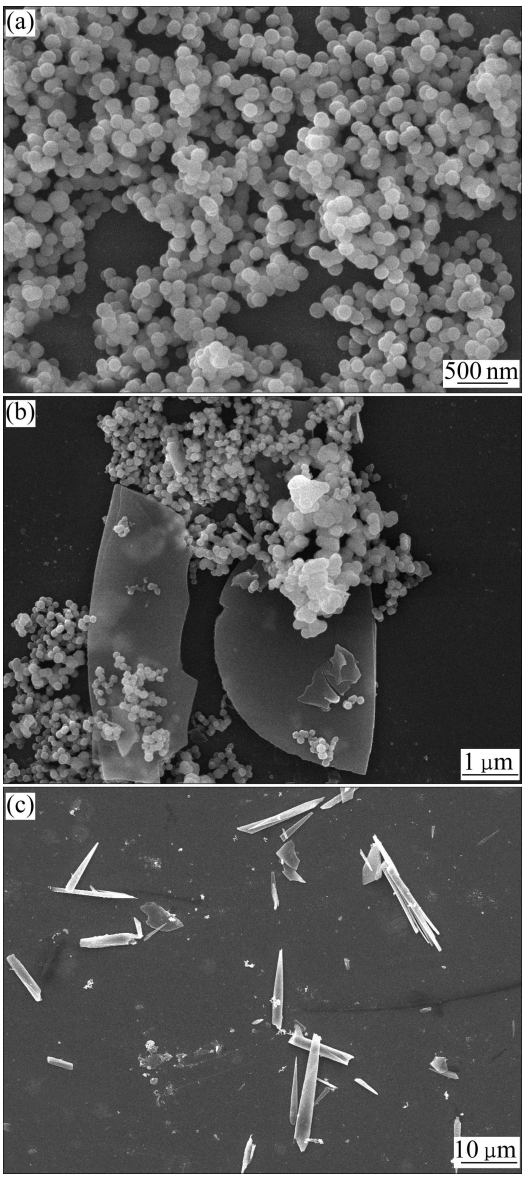

Fig. 1 FE-SEM micrographs showing morphologies of three typical precursors: (a) Submicron spheres (R=10); (b) Mixtures of submicron spheres and microplates (R=20); (c) Microplates (R=60)

shown in Fig. 1(c), for the product obtained at R=60. At R=20, the product is a mixture of the submicron spheres and the microplates (Fig. 1(b)), indicating that they are on the way of morphology transformation.

Figure 2 shows the XRD patterns for two representative samples of the submicron spheres (R=10) and the microplates (R=60). The submicron spheres are essentially amorphous, similar to $Y(OH)CO_3$ made by MATIJEVIĆ and HSU [17]. The microplates can be nearly indexed to the orthorhombic structured yttrium carbonate hydrate phase ($Y_2(CO_3)_3{\cdot}3H_2O$, JCPDS file No. 25—1010), except for changed relative intensities of the diffraction peaks due to a textured distribution of the microplates on the glass holder for XRD analysis.

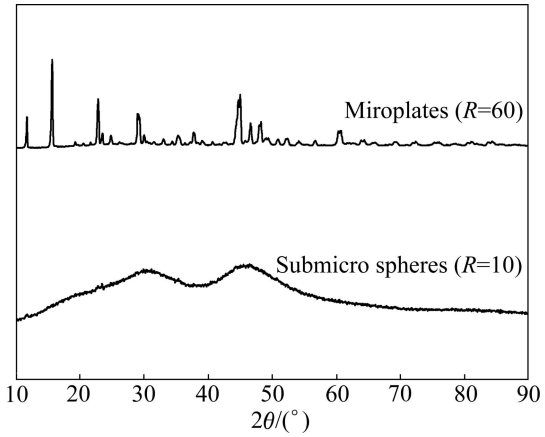

Fig. 2 XRD patterns for two typical precursors of submicron spheres (R=10) and microplates (R=60)

Chemical compositions of the above two samples can be further confirmed by FT-IR (Fig. 3). Indeed, the amorphous spheres exhibit a spectral characteristic of the lanthanide basic carbonate hydrate ($Ln(OH)CO_3{\cdot}H_2O$) monospheres classically made via urea-based homogeneous precipitation [7,8]. The strong and broad absorption bands in the region of 3000−3500 cm^{-1} (peaked at ~3315 cm^{-1}) and the shoulder near 1655 cm^{-1} provide evidence for water of hydration in the structure or surface adsorbed water, and they are assignable to the O—H stretching vibrations (ν_1 and ν_3) and H—O—H bending mode (ν_2), respectively [18,19]. The absorption band observed in the region of 3500− 3750 cm^{-1} (centered at ~3536 cm^{-1}) is indicative of hydroxyl (OH^- groups [18,19]. The presence of carbonate ions in the molecular structure is confirmed by the appearance of absorption doublets in the region of 1350− 1600 cm^{-1} (ν_3 of CO_3^{2-}, peaked at ~1415 and 1527 cm^{-1}) and also by the occurrence of the absorption at ~2362 cm^{-1} and the multiple absorptions ranging from 500− 1000 cm^{-1} (ν_2 and ν_4 of CO_3^{2-}) [18,19]. The microplates similarly show

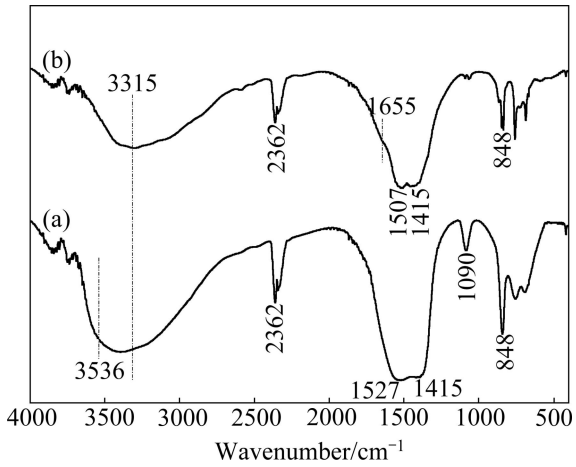

Fig. 3 FT-IR spectra for two typical precursors of submicron spheres (R=10) (a) and microplates (R=60) (b)

the water of hydration band at ~3315 cm^{-1} and the CO_3^{2-} bands but lack the absorption by OH^- at 3536 cm^{-1}, suggesting a hydrated normal carbonate for the microplates as revealed by XRD.

The chemical composition of a hydrothermal product is the result of competition among the anionic species in combining with cations, and the final composition would always have the lowest solubility to minimize the free energy of the system. Though the soluble products of the basic carbonate and normal carbonate are not available to us, there is no doubt to say that they are the most stable forms under their respective hydrothermal conditions. The hydrolysis of urea yields ammonia and carbonate ions, and thus a higher molar ratio of urea to Y+Eu would give a higher solution pH and more CO_3^{2-}. It is also known that CO_3^{2-} tends to stabilize in a more alkaline solution. These may account for the formation of the normal carbonate at the high molar ratio of urea to Y+Eu of R=40−100. At even higher R values, a yttrium ammine carbonate ($NH_3{\cdot}Y_2(CO_3)_3{\cdot}3H_2O$) phase might be obtained, as inferred from the work of MATIJEVIĆ and HSU [17].

3.2 Shape-dependent crystallization and luminescence of $(Y_{0.95}Eu_{0.05})_2O_3$ submicron spheres and microplates

Figure 4 shows the typical FE-SEM images of the $(Y_{0.95}Eu_{0.05})_2O_3$ calcined at 1000 °C for 4 h. Clearly, the resultant oxides largely retain the original morphologies of their respective precursors except for a slight shrinkage in particle size by annealing. The calcination products have displayed all the characteristic diffractions corresponding to the cubic structured Y_2O_3 (space group: $Ia\bar{3}$ (206), JCPDS: 89—5591), as shown in Fig. 5. The morphology confined crystal growth was observed for the microplates. These two samples have their respective

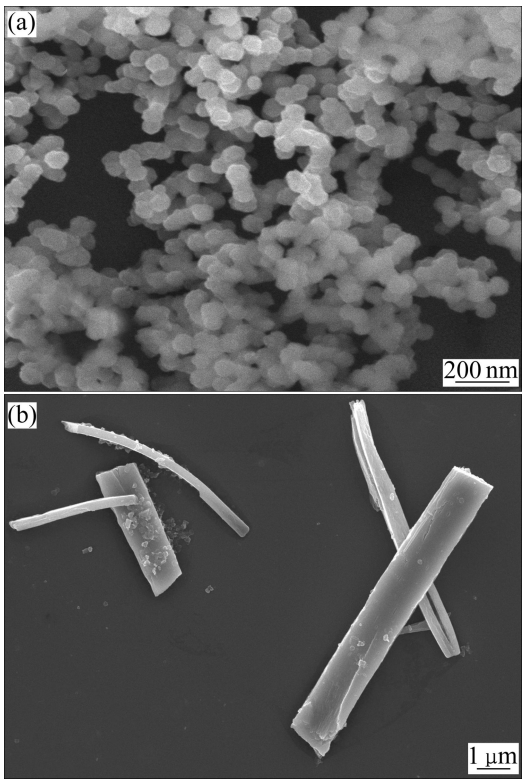

Fig. 4 FE-SEM micrographs showing morphologies of $(Y_{0.95}Eu_{0.05})_2O_3$ oxides calcined from submicron spheres (R=10) (a) and microplates (R=60) (b) at 1000 °C for 4 h

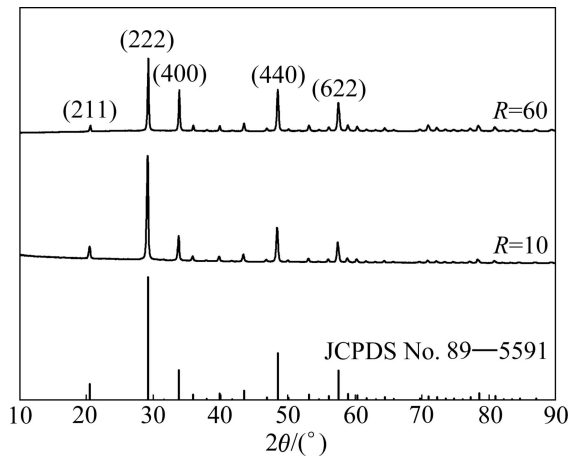

Fig. 5 XRD patterns of $(Y_{0.95}Eu_{0.05})_2O_3$ oxides calcined from submicron spheres (R=10) and microplates (R=60) at 1000 °C for 4 h

(400)/(222) intensity ratios of ~25.4% (submicron sphere) and 58.9% (microplate), against a value of 24.6% from the data file. The obvious change of the (400)/(222) intensity ratio for the microplates indicates that Y_2O_3:Eu^{3+} nucleates within the microplates along with the thermal decomposition of the carbonate precursor but the subsequent free growth of the oxide nuclei is significantly restricted by the two-dimensional plate-like morphology [16]. As the (222) and (400) planes have a dihedral angle of ~54.7º and the microplates tend to lie parallel to the surface of the glass holder during XRD analysis, the substantially higher (400)/(222) intensity ratio thus implies an enhanced exposure of the (400) facets on plate surfaces.

It is widely observed that Y_2O_3:Eu^{3+} phosphors show a typical photoluminescence excitation band at ~250 nm, and are ascribed to the electronic transition from the 2p orbital of O^{2-} to the 4f orbital of Eu^{3+} [7−16, 20, 21]. Under UV excitation at 250 nm, the Y_2O_3:Eu^{3+} spheres and plates calcined at 1000 °C for 4 h exhibit PL bands at essentially identical positions. As marked in Fig. 6, all the emission bands observed at 583, 589−601, 613, and 652 nm can be assigned to the $^5D_0\rightarrow{}^7F_J$ (J = 0, 1, 2, 3) transitions of Eu^{3+}, respectively. The cubic Y_2O_3 lattice is known to have two different types of crystallographic positions for Eu^{3+} substitution: the 24d site with C_2 symmetry and the 8b site with S_6 inversion symmetry [22,23]. It is well known that the $^5D_0\rightarrow{}^7F_2$ electric dipole transition is hyper-sensitive to the local environment of Eu^{3+} ions [23−25]. The intensity ratio of $^5D_0\rightarrow{}^7F_2$ transition (monitored at 613 nm) to $^5D_0\rightarrow{}^7F_1$ transition (monitored at 595 nm), called asymmetry factor, has been widely used as a very sensitive and efficient probe to detect the local structure around Eu^{3+}. In our present work, both the samples have similar asymmetry factors of ~11.0, indicating that the local symmetries of Eu^{3+} in Y_2O_3 do not vary significantly between the two morphologies.

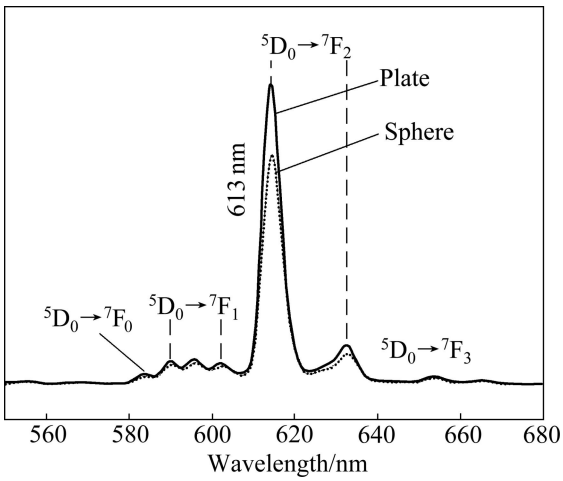

Fig. 6 Emission spectra of $(Y_{0.95}Eu_{0.05})_2O_3$ red phosphors calcined at 1000 °C for 4 h under 250 nm excitation

The strongest emission peak near 613 nm is due to the forced electric dipole $^5D_0\rightarrow{}^7F_2$ transition of Eu^{3+}. Taking the 613 nm emission for comparison, the microplates show an intensity of ~1.33 times that of the

submicron spheres. The microplates have a larger particle size and thus a denser packing of the primary phosphor crystallites compared with the submicron spheres, which allows a less scattering of the evolved light and hence a stronger luminescence.

4 Conclusions

1) Red-emission $(Y_{0.95}Eu_{0.05})_2O_3$ submicron spheres and microplates were selectively processed via hydrothermal precursor synthesis (150 °C, 12 h) followed by calcination at 1000 °C, without using any surfactant, catalyst, or template.

2) The precursor would change from $(Y_{0.95}Eu_{0.05})$-$(OH)CO_3 \cdot H_2O$ monospheres to $(Y_{0.95}Eu_{0.05})_2(CO_3)_3 \cdot 3H_2O$ microplates along with an increase in the molar ratio of urea to Y+Eu from 10 to 40−100.

3) Morphology confined crystal growth was observed for the microplates, inducing more (400) facets exposed on plate surfaces.

4) Under UV excitation at 250 nm, the $(Y_{0.95}Eu_{0.05})_2O_3$ submicron spheres and microplates exhibit nearly identical positions of the PL bands and similar asymmetry factors (~11.0) of luminescence but the latter shows a significantly strong red emission at ~613 nm, which was ascribed to the lager particle size and denser packing of primary phosphor crystallites of the microplates.

References

[1] EKAMBARAM S, PATIL K C, MAZZA M. Synthesis of lamp phosphors: Facile combustion approach [J]. J Alloys Compd, 2005, 393: 81−92.

[2] KITYK I V, NYK M, STREK W, JABLONSKI J M, MISIEWICE J. Circularly photostimulated electrogyration in europium- and terbium-doped GaN nanocrystals embedded in a silica xerogel matrix [J]. J Phys Condens Matter, 2005, 17: 5235−5245.

[3] LENGGORO I W, ITOH Y, OKUYAMA K. Nanoparticles of a doped oxide phosphor prepared by direct-spray pyrolysis [J]. J Mater Res, 2004, 19: 3534−3539.

[4] KANG Y C, ROH H S, PARK S B. Preparation of Y_2O_3:Eu phosphor particles of filled morphology at high precursor concentrations by spray pyrolysis [J]. Adv Mater, 2000, 12: 451−453.

[5] KANG Y C, ROH H S, PARK S B. Sodium carbonate flux effects on the luminescence characteristics of $(Y_{0.5}Gd_{0.5})_2O_3$:Eu phosphor particles prepared by spray pyrolysis [J]. J Am Ceram Soc, 2001, 84: 447−449.

[6] CAMENZIND A, STROBEL R, KRUMEICH F, PRATSINIS S E. Luminescence and crystallinity of flame-made Y_2O_3:Eu^{3+} nanoparticles [J]. Adv Powder Technol, 2007, 18: 5−22.

[7] LI J G, LI X D, SUN X D, ISHIGAKI T. Monodispersed colloidal spheres for uniform Y_2O_3:Eu^{3+} red-phosphor particles and greatly enhanced luminescence by simultaneous Gd^{3+} doping [J]. J Phys Chem C, 2008, 112: 11707−11716.

[8] WANG H, LIN C K, LIN J, YU M. Monodisperse spherical core-shell-structured phosphors obtained by functionalization of silica spheres with Y_2O_3:Eu^{3+} layers for field emission displays [J]. Appl Phys Lett, 2005, 87: 181907.

[9] WANG H, YU M, LIN C K, LIN J. Synthesis and luminescence properties of monodisperse spherical Y_2O_3:Eu^{3+}@SiO_2 particles with core−shell structure [J]. J Phys Chem C, 2007, 111: 11223−11230.

[10] WU C F, QIN W P, QIN G S. Photoluminescence from surfactant-assembled Y_2O_3:Eu nanotubes [J]. Appl Phys Lett, 2003, 82: 520−522.

[11] ZHANG J L, HONG G Y. Synthesis and photoluminescence of the Y_2O_3:Eu^{3+} phosphor nanowires in AAO template [J]. J Solid State Chem, 2004, 177: 1292−1296.

[12] WAN J X, WANG Z H, CHEN X Y, MU L Y, QIAN Y T. Shape-tailored photoluminescent intensity of red phosphor Y_2O_3:Eu^{3+} [J]. J Cryst Growth, 2005, 284: 538−543.

[13] HE Y, TIAN Y, ZHU Z F. Large-scale synthesis of luminescent Y_2O_3:Eu nanobelts [J]. Chem Lett, 2003, 32: 862−863.

[14] WU X, TAO Y, GAO F, DONG L, HU Z. Preparation and photoluminescence of yttrium hydroxide and yttrium oxide doped with europium nanowires [J]. J Cryst Growth, 2005, 277: 643−649.

[15] LU Z G, QIAN D, TANG Y G. Facile synthesis and characterization of sheet-like Y_2O_3:Eu^{3+} microcrystals [J]. J Cryst Growth, 2005, 276: 513−518.

[16] ZHU Q, LI J G, LI X D, SUN X D. Morphology dependent crystallization and luminescence behaviors of $(Y,Eu)_2O_3$ red phosphors [J]. Acta Mater, 2009, 57: 5975−5985.

[17] MATIJEVIĆ E, HSU W P. Preparation and properties of monodispersed colloidal paticles of lanthanide compounds (1): Gadolinium, europium, terbium, samarium, and cerium (III) [J]. J Colloid Interface Sci, 1987, 118: 506−523.

[18] NAKAMOTO K. Infrared spectra of inorganic & coordination compounds [M]. New York: John Wiley & Sons, 1963.

[19] GADSDEN J A. Infrared spectra of minerals and related inorganic compounds [M]. Newton, MA: Butterworth, 1975.

[20] ZHANG Ming, LI Xin-hai, WANG Zhi-xing, HU Qi-yang, GUO Hua-jun. Synthesis of Y_2O_3:Eu^{3+} phosphors by surface diffusion and their photoluminescence properties [J]. Transactions of Nonferrous Metals Society of China, 2010, 20(11): 115−118.

[21] HUANG Yan, YE Hong-qi, ZHUANG Wei-dong, HU Yun-sheng, ZHAO Chun-lei, LI Cui, GUO Song-xia. Preparation of Y_2O_3:Eu^{3+} phosphor by molten salt assisted method [J]. Transactions of Nonferrous Metals Society of China, 2007, 17(3): 644−648.

[22] BLASSE G, GRABMAIR B C. Luminescent materials [M]. Berlin: Springer Verlag, 1994.

[23] PAPPALARDO R G, HUNT R B Jr. Dye-laser spectroscopy of commercial Y_2O_3:Eu^{3+} phosphors [J]. J Electrochem Soc, 1985, 132: 721−730.

[24] JUDD B R. Optical Absorption intensities of rare-earth ion [J]. Phys Rev, 1962, 127: 750−761.

[25] OFELT G S. Intensities of crystal spectra of rare-earth ions [J]. J Chem Phys, 1962, 37: 511−520.

$(Y_{0.95}Eu_{0.05})_2O_3$亚微米球、微米板片的选择合成及荧光性能的形貌依存性

朱　琦，李继光，胥 永，李晓东，孙旭东

东北大学 材料各向异性与织构教育部重点实验室，沈阳 110819

摘　要：采用先水热合成 (150 °C, 12 h)、后煅烧(1000 °C)来实现$(Y_{0.95}Eu_{0.05})_2O_3$亚微米球形和微米板片红色荧光颗粒的形貌可控合成。通过 XRD、FT-IR、FE-SEM 和 PL 等检测手段对样品进行分析。结果表明：将尿素与 Y+Eu 的摩尔比由 10 增大至 40~100，得到的前驱体由碱式碳酸盐亚微米球转变为碳酸盐微米片；经 1000 °C 煅烧所得氧化物能够继承前驱体的形貌特征；板片二维形貌的限制内部晶粒自由生长，使更多的(400)晶面暴露在板片颗粒表面；在 250 nm 紫外光的激发下，荧光颗粒的荧光发射峰位及荧光不对称因子[$I(^5D_0\rightarrow{}^7F_2)/I(^5D_0\rightarrow{}^7F_1)$, ~11]均与颗粒形貌的相关性不强，但荧光强度呈现明显的形貌依存性；微米板片颗粒的尺寸大，从而其比表面积小，因此具有更高的荧光强度(微米板片在~613 nm 处的荧光强度为球形颗粒的~1.33 倍)。

关键词：发光材料；粉体合成；物理性能的形貌依存性；稀土；光谱学

(Edited by LI Xiang-qun)